Between phase and amplitude oscillators

Pau Clusella[1,2] and Antonio Politi[1]

[1]*Institute for Complex Systems and Mathematical Biology, SUPA,*
University of Aberdeen, Aberdeen AB24 3UE, United Kingdom
[2]*Dipartimento di Fisica, Università di Firenze, I-50019 Sesto Fiorentino, Italy*
(Dated: January 31, 2019)

We analyze an intermediate collective regime where amplitude oscillators distribute themselves along a closed, smooth, time-dependent curve $\mathcal{C}$, thereby maintaining the typical ordering of (identical) phase oscillators. This is achieved by developing a general formalism based on two partial differential equations, which describe the evolution of the probability density along $\mathcal{C}$ and of the shape of $\mathcal{C}$ itself. The formalism is specifically developed for Stuart-Landau oscillators, but it is general enough to be applied to other classes of amplitude oscillators. The main achievements consist in: (i) identification and characterization of a new transition to self-consistent partial synchrony (SCPS), which confirms the crucial role played by higher Fourier harmonics in the coupling function; (ii) an analytical treatment of SCPS, including a detailed stability analysis; (iii) the discovery of a new form of collective chaos, which can be seen as a generalization of SCPS and characterized by a multi-fractal probability density. Finally, we are able to describe given dynamical regimes both at the macroscopic as well as the microscopic level, thereby shedding further light on the relationship between the two different levels of description.

I. INTRODUCTION

One of the peculiarities of high-dimensional complex systems is the spontaneous emergence of nontrivial dynamical regimes over multiple scales. The simultaneous presence of a macroscopic and a microscopic dynamics in mean-field models is perhaps the simplest instance of this phenomenon and, yet, it is not fully understood. It is, for instance, not clear how and to what extent the microscopic and macroscopic world are related to one another; even the minimal properties required for the emergence of a non trivial collective dynamics are unknown [1]. This difficulty is not a surprise, as the problem is akin to the emergence of different thermodynamic phases in equilibrium statistical mechanics, a crucial difference being that there are no Boltzmann-Gibbs weights to be invoked and, moreover, the thermodynamic phases themselves are not steady.

A research area where these problems are particularly relevant is that of multicomponent oscillatory systems, such as those encountered in dealing with chemical reactions (see, e.g. the emergence of glycolytic oscillations in yeast cells [2] or the synchronization of coupled chemical oscillators [3]), mechanical oscillators [4]; waveguide [5] and semiconductor [6] laser arrays, grids of Josephson junctions [7], and include even social phenomena (see e.g., egg-laying in sea bird colonies [8]). In some cases the collective behavior is expected to be periodic (see e.g. heart pacemaker cells [9]). In others, the dynamics must be irregular since fluctuations encode to-be-processed information, as in the electrical activity within the mammalian brain, where populations of neurons collectively contribute to determining meaningful signals.

In the absence of a general theory to assess the properties of the collective dynamics from those of microscopic models, it is natural and desirable to concentrate on relatively simple setups, where chances to derive general laws are higher. More specifically, in this paper we consider populations of identical deterministic oscillators. In spite of the strong simplifications, it is not yet clear under which conditions a rich collective dy-namics is expected to arise.

Generally speaking, collective regimes in mean-field models can be classified into two large families: (i) symmetry-broken phases, where the ensemble elements split in two or more groups, each characterized by its own dynamics; (ii) symmetric phases, where all oscillators behave in the same way. Clustered [10] and chimera [11, 12] states are the two most prominent examples of the former type, while fully synchronous and splay states are the simplest examples of the latter one. In this paper we focus on the latter class and, more precisely, on the emergence of collective chaos, our goal being to shed light on the way macroscopically active degrees of freedom may spontaneously emerge in an ensemble of identical units.

In general, it is natural to classify the different setups according to the dynamical complexity of the single oscillators, since the overall behavior should be ultimately traced back to the rules determining the evolution of the single elements. Intrinsically chaotic elements such as logistic maps sit at the top of the hierarchy. It is known since many years that collective chaos may sponentaneously emerge as a result of subtle correlations among the single dynamical units [13]. Collective chaos can emerge also in periodic oscillators such as the Stuart-Landau model [14–16], since the macroscopic mean field can trigger and maintain a microscopic chaos, thereby giving rise to a regime similar to the previous one.

By further descending the ladder of the single-unit complexity, no evidence of collective chaos has been found in mean-field models of identical phase-oscillators, but no rigorous argument excluding that this can happen is available. In fact, in all mean-field systems of identical oscillators, the probability distribution satisfies a self-consistent functional equation which, being nonlinear and infinite-dimensional can in principle give rise to a chaotic dynamics. Nevertheless, collective chaos in phase oscillators has been found only when either delayed interactions [17], multiple populations [18], or heterogeneity [19] is included in the model. Otherwise, at most macroscopic periodic oscillations arise (the so-called

self-consistent partial synchrony SCPS) [20–25], the simplest setup for their observation being the biharmonic Kuramoto-Daido model [26]. The so-called balanced regime observed in the context of neural networks is, instead, an entirely different story, since the collective dynamics is basically the result of the amplification of microscopic fluctuations [27].

Altogether, new theoretical approaches are required to improve our general understanding of the collective behavior of ensembles of dynamical units. In phase oscillators characterized by strictly sinusoidal coupling-functions (Kuramoto type) the Watanabe-Strogatz theorem [28] and the Ott-Antonsen Ansatz [29] imply that no more than three collective degrees of freedom can emerge. What can we say in more general contexts? In this paper, we discuss an intermediate regime, where amplitude oscillators (characterized by at least two variables) retain a key property of phase oscillators, *i.e.* they can be parametrized by a single phase-like variable. In practice, the amplitude dynamics is sufficiently stable to force the oscillators towards a smooth closed curve $\mathcal{C}$ such as in standard phase oscillators, but not stable enough to prevent fluctuations of the curve itself, which therefore acts as an additional source of complexity. We refer to this regime, which has been so far basically overlooked, as to Quasi Phase Oscillators (QPO). We are only aware of a preliminary study carried out by Kuramoto & Nakagawa, who performed microscopic simulations of an ensemble of Stuart-Landau oscillators [30]. Here we develop a general formalism, which allows describing QPO at a macroscopic level. As a result, we are able to identify and describe a series of dynamical regimes ranging from plain SCPS to a new type of collective chaos. SCPS itself is already an intriguing regime. In fact, under the action of a self-consistent mean field, the single oscillators exhibit generically a quasiperiodic behavior without phase locking (no Arnold tongues). Said differently, the transversal Lyapunov exponent of each single oscillator (conditioned to a given "external" forcing) is consistently equal to zero, when a control parameter is varied. The hallmark of QPO is that the transverse Lyapunov exponent is not positive, even when the "external" mean-field forcing is chaotic: actually, it is even slightly negative, implying that the phase probability distribution is not smooth but multifractal. This is at variance with the "standard" collective chaos observed in a different parameter region of the Stuart-Landau model [14–16, 31], characterized by a positive transversal Lyapunov exponent.

In Section II we introduce the model and develop the formalism, which consists in the derivation of two partial differential equations (PDEs), one describing the probability density of the oscillators along the curve $\mathcal{C}$ and the other describing the shape of the curve itself. These equations are thereby simulated to identify the different regimes: the agreement with the integration of the microscopic equations validates the whole approach. Next, an exact stability analysis of the splay state is performed in Section III, which allows determining the critical value of the coupling strength where SCPS is born. Section IV is devoted to the analysis of SCPS, leading to an exact solution for the distribution of phases and for the shape of $\mathcal{C}$. Therein we analyze also the transition to SCPS, uncovering very subtle properties: superficially, the transition

corresponds to the critical point of the Kuramoto-Sakaguchi model [32], which separates the stability of the splay state from that of the synchronous solution. However, this is not entirely correct, as it is known that the Kuramoto-Sakaguchi model cannot support SCPS. In fact, it turns out that the mutual coupling and, in particular, the fluctuations of the curve $\mathcal{C}$, give birth to higher Fourier harmonics, which are essential for the stabilization of SCPS. In the following section V, we analyze the increasingly complex regimes generated when the coupling is further increased. In particular, we see that the transition to chaos is rather anomalous: a sort of intermediate scenario between the standard low-dimensional route to chaos where a single exponent becomes positive, and high-dimensional transitions when the number of unstable directions is proportional to the system size. In the present context, we have evidence of the simultaneous appearance of three positive exponents, irrespective of the number of oscillators. An additional unusual feature of the chaotic dynamics is the presence of (infinitely many) nearly zero exponents, which, according to the Kaplan-York formula, make the system high dimensional in spite of the finite (and small) number of unstable directions. In section V we discuss also macroscopic and microscopic Lyapunov exponents, showing that they are consistent with one another. This equivalence is far from trivial, since in all previous instances of collective chaos the correspondence between the two spectra was at most restricted to very few exponents, the reason for the difference being that while the microscopic exponents refer to perturbations of single trajectories, the macroscopic ones refer to perturbations of the distributions of phases. In section VI we provide evidence of the ubiquity of QPOs and validate the generality of the the the macroscopic description developed in section II by studying an ensemble of globally coupled Rayleigh oscillators. Finally, section VII contains a summary of the main results and of the open problems.

II. THE MODEL

Following Ref. [14], we consider an ensemble of N coupled Stuart-Landau oscillators

$$\dot{z}_j = K(1 + ic_1)(\bar{z} - z_j) + z_j - (1 + ic_2)|z_j|^2 z_j \qquad (1)$$

where $z \in \mathbb{C}$ and

$$\bar{z} = \frac{1}{N} \sum_{m=1}^{N} z_m$$

is the mean field. The formulation of Refs. [15, 16] is recovered by setting $t \to Kt$, $\alpha = c_2$, $\eta = c_1$ and $\mu = K^{-1}$.

A homogeneous system of globally coupled oscillators such as (1) can display two types of stationary solutions: a state of *full synchrony* and *incoherent states*. In the state of full synchrony all the oscillators evolve periodically as $z_j = \bar{z} = e^{ic_2 t}$. Incoherent states correspond to a distribution of oscillators such that the mean field $\bar{z}$ vanishes. There are infinitely many ways of realizing an incoherent state, the
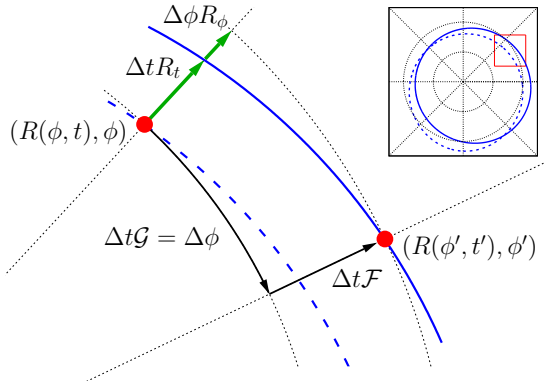
FIG. 1. Schematic representation of the phase parametrization of $\mathcal{C}$ and its time evolution. Dashed blue curve depicts the shape of of $\mathcal{C}$ at time t, whereas the continuous blue line indicates the position of $\mathcal{C}$ at time $t' = t + \Delta t$. The inset shows a zoom out version, with the red rectangle indicating the zone depicted in the main figure.

simplest being a completely homogeneous distribution of the phases along a circle (of radius $\sqrt{1-K}$) also known as *splay state*.

For small coupling strength $K \ll 1$, the model can be mapped onto a Kuramoto-Sakaguchi model [25], which is known to give rise only to either fully synchronous or splay states. For larger coupling strength, the model displays a rich variety of dynamics, including clustered states, chimera states, and different forms of collective chaos [14–16, 30, 33]. In particular, Nakagawa & Kuramoto [30] reported numerical evidence of a dynamical regime where the oscillators seem to be distributed along a smooth time-dependent closed curve. In this paper, we revisit such a behavior, developing a formalism, which can, in principle, be applied to generic ensembles of mean-field driven amplitude oscillators.

A general macroscopic formulation of system (1) requires the knowledge of the probability density on the complex plane $Q = Q(z,t)$. Nevertheless, if the amplitude dynamics is sufficiently stable, the oscillator variables naturally converge and are eventually confined to a closed curve $\mathcal{C}$.

Whenever this is the case, the probability density is restricted to a unidimensional curve $\mathcal{C}$ and thus can be parametrized by a phase-like variable, which represents the position along $\mathcal{C}$ itself. At the same time, the shape of the curve is expected to vary over time, this phenomenon being a a manifestation of amplitude dynamics. In principle, so long as a proposed definition of the phase allows distinguishing all points along the curve at all times, it allows for a faithful reconstruction of the collective dynamics. For computational purposes, it is convenient to deal with simple structures for the velocity field. In the case of the Stuart-Landau oscillators it is natural and sufficient to represent z in polar coordinates and thereby parametrize $\mathcal{C}$ by expressing the radius $R(\phi,t)$ as a function of the phase ϕ. Accordingly the probability density can be written as

$$Q(z,t) = Q(z,t)\delta(|z| - R(\phi,t)) =: P(\phi,t).$$

The meaningfulness of this approach is verified a posteriori

by the consistency of the theoretical predictions and by the agreement with direct numerical simulations.

Our first goal is to derive the evolution equations for R and P. In order to do so, it is convenient to express Eq. (1) in polar coordinates, $z = r\, e^{i\phi}$,

$$\dot{r}_j = \mathcal{F}[r_j, \phi_j, \overline{z}]$$
$$\dot{\phi}_j = \mathcal{G}[r_j, \phi_j, \overline{z}] \,,$$

where

$$\mathcal{F}[r, \phi, \overline{z}] = (1 - K - r^2)r + K\,\mathrm{Re}[(1 + ic_1)\overline{z}\,e^{-i\phi}]$$
$$\mathcal{G}[r, \phi, \overline{z}] = -c_1 K - c_2 r^2 + \frac{K}{r}\,\mathrm{Im}[(1 + ic_1)\overline{z}\,e^{-i\phi}] \,.$$

Let us now consider a time interval $\Delta t \ll 1$ and $t' = t + \Delta t$. At time t the oscillator with index j has polar coordinates $[r_j(t), \phi_j(t)] \equiv [R(\phi,t), \phi]$ while at time t' is in $[r_j(t'), \phi_j(t')] \equiv [R(\phi',t'), \phi']$, as indicated in Fig. 1. By then expanding $r_j(t')$ and $\phi_j(t')$ around t, one can write

$$\begin{cases} R(\phi', t') \approx R(\phi,t) + \Delta t\,\mathcal{F}[R(\phi,t), \phi, \overline{z}] \\ \phi' = \phi + \Delta t\,\mathcal{G}[R(\phi,t), \phi, \overline{z}] \,, \end{cases}$$

where we have assumed a smooth dependence of R on ϕ and expanded it around ϕ' (notice that throughout the paper we use the notation $f_x := \frac{\partial f}{\partial x}$). In the limit of $\Delta t \to 0$,

$$\frac{\partial R}{\partial t}(\phi, t) = \mathcal{F}[R, \phi, \overline{z}] - \mathcal{G}[R, \phi, \overline{z}]R_\phi \,. \tag{2}$$

On the other hand, the evolution of P is determined by the angular flux at $r = R(\phi,t)$,

$$\frac{\partial P}{\partial t}(\phi, t) = -\frac{\partial}{\partial \phi}\Big\{P(\phi,t)\mathcal{G}[R, \phi, \overline{z}]\Big\}. \tag{3}$$

The mean field is finally defined as

$$\overline{z}(t) = \int_0^{2\pi} P(\phi,t)R(\phi,t)e^{i\phi}d\phi. \tag{4}$$

From the expression for $\mathcal{G}[R, \phi, \overline{z}]$, one can recognize the Kuramoto-Sakaguchi structure [32] of the velocity field, with however, the important difference of the additional factor $R(\phi,t)$ in the definition of the order parameter. We will see that the time dependence of $R(\phi,t)$ (it obeys a distinct differential equation) enriches the complexity of the collective dynamics.

Overall, equations (2,3,4) represent a system of two nonlinear Partial Differential Equations (PDEs) describing the macroscopic behavior of the oscillators whenever they are spread along a closed phase-parameterized smooth curve.

Such a system can be solved numerically by means of a split-step Fourier or pseudospectral method [34]. The algorithm consists in expanding R and P spatially in Fourier

space,

$$P(\phi, t) = \frac{1}{2\pi} \sum_{k=-\infty}^{\infty} \tilde{P}(k, t) e^{-ik\phi} \quad \text{and}$$

$$R(\phi, t) = \frac{1}{2\pi} \sum_{k=-\infty}^{\infty} \tilde{R}(k, t) e^{-ik\phi}$$

where

$$\tilde{P}(k, t) = \int_0^{2\pi} d\phi \; P(\phi, t) e^{ik\phi} \quad \text{and}$$

$$\tilde{R}(k, t) = \int_0^{2\pi} d\phi \; R(\phi, t) e^{ik\phi}.$$

By truncating the Fourier series for a large enough wavelength M, one can then integrate in time the different Fourier modes $\tilde{P}(k, t)$ and $\tilde{R}(k, t)$ using a standard method for ordinary differential equations. Since the computation of a nonlinear term of order q in Fourier space requires $\mathcal{O}(M^q)$ operations, it is more convenient to compute the velocity fields in real space instead. In fact, by invoking fast Fourier transform (FFT) algorithms, the computational cost of the nonlinear fluxes reduces to $\mathcal{O}(4n \log(2n))$, where n is the number of points of the real support. We use a fourth-order Runge-Kutta integration method with time step δt, set to 10^{-3} in most of the simulations. In order to avoid aliasing errors in the successive calls of the FFT we use the 3/2-truncation rule using a real spatial grid of $n = 2048$ points and a truncation of $M = 680$ in the Fourier expansion. Nevertheless, in the presence of chaotic dynamics (see below) the numerics become more challenging and it is necessary to increase both spatial and temporal resolutions. Therefore, for $K > 0.416$ we use $M = 1024$ and $\delta t = 0.5 \cdot 10^{-3}$, and keep $n = 2048$. In this case it is necessary to introduce a smoothing technique to prevent the growth of the aliasing errors. Thus we add a small diffusive term in equation (3),

$$\frac{\partial P}{\partial t}(\phi, t) = -\frac{\partial}{\partial \phi} \left\{ P(\phi, t)\mathcal{G}[R, \phi, \bar{z}] \right\} + D\frac{\partial^2}{\partial \phi^2} P(\phi, t) \; .$$

A diffusion level of $D = 10^{-8}$ is enough to stabilize the algorithm while preserving the dynamical properties of the system.

In order to double check our numerics we have fixed two parameters as in Ref. [30] ($c_1 = -2$ and $c_2 = 3$) and treated the coupling strength K as the leading control parameter. The results of our numerical simulations are reported in figures 2, 3 and 4. In figure 2 we show the time-average of the mean-field $|\bar{z}|$ computed both using the microscopic formulation of the system (1) with $N = 4096$ (black plusses) and using the macroscopic equations solved with the pseudospectral method (red circles). The nice agreement confirms the correctness of the macroscopic equations.

The behavior of the order parameter unveils a series of bifurcations across various dynamical regimes, marked with vertical dashed black lines. In figure 3 we show the time

evolution of the order parameter modulus $|\bar{z}|$ for different values of K, each belonging to a different dynamical regime. In the top panels of figure 4 we plot snapshots of R (black dashed lines) and the corresponding probability densities P (red lines). While the shape of the curve $\mathcal{C}$ remains very smooth when the coupling is increased, the probability profiles become increasingly rugged, revealing an increasing contribution of higher Fourier modes. This is better appreciated by looking at the middle row panels of Fig. 4, where the corresponding Power Spectral Density (PSD) is reported in a logarithmic scale (same color code for the different curves). For comparison, two snapshots of the corresponding microscopic simulations are displayed in the bottom panels (see red squares and blue circles in figure 4(a3),(b3),(c3), and (d3)).

For $K < K_1 \approx 0.4123$, the oscillators are uniformly distributed on a perfect circle and the mean-field $\bar{z}$ vanishes, *i.e.*, the system is in a *splay state*. For $K = K_1$ there is a first transition to a regime where the mean-field dynamics is a pure periodic rotation on a one-dimensional torus (T1), accompanied by a quasiperiodic dynamics of the single oscillators. This regime is therefore an example of *self-consistent partial synchrony* (SCPS) first uncovered in a model of leaky integrate-and-fire neurons [20] and fully described in biharmonic Kuramoto-Daido oscillators [26]. In this regime, the mean-field modulus is constant (see red line in Fig. 3). In fact, both P and R are spatially nonuniform steady functions if observed in a suitably rotating frame (see Fig. 4(a1), where we can also notice that the shape is dominated by a few long wavelength modes - panel (a2)). At $K = K_2 \simeq 0.4138$ a macroscopic Hopf bifurcation occurs, which introduces a second frequency. As a result, the collective dynamics is quasiperiodic (T2, but periodic, if observed in a suitably rotating frame) (see the blue line in Fig. 3). Now the shape of P and R fluctuate in time and more Fourier modes contribute (see figures 4(b1), (b2), and (b3)).

At $K = K_3 \simeq 0.41588$, yet another frequency adds to the macroscopic dynamics, although indistinguishable from the average value of the order parameter. Thus, as better argued in the following, the dynamics of the order parameter becomes three-dimensional (T3) (see the green line in Fig. 3). The shape of P becomes more uneven, with several bumps that evolve on time, and the spatial spectra involve higher Fourier modes (see Fig. 4(c1),(c2), and (c3)).

The T3 regime is stable for a small range of the parameter value; beyond $K = K_4 \simeq 0.41605$ the system becomes chaotic. Although R keeps being quite smooth, the shape of P occasionally develops several peaks that become sharper upon increasing the coupling strength (see Fig. 4(d1) and (d2)). Such peaks correspond to quasi-cluster structures in the microscopic simulations (see Fig. 4(d3)) and generate spurious ringing artifacts that eventually lead to numerical instabilities. Nevertheless, as explained before, increasing the numerical resolution and introducing a negligible diffusion, one can accurately integrate the macroscopic equations for long times.

For yet larger K values, the order parameter vanishes after a long chaotic transient. However, the asymptotic regime is
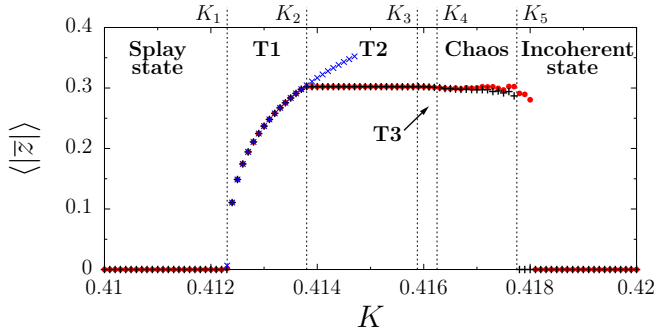
FIG. 2. Time-averaged mean-field $\langle|\bar{z}|\rangle$ for different values of the coupling strength K and fixed $c_1 = -2$ and $c_2 = 3$. Black plusses show the results from microscopic simulations of the system as given by (1) with $N = 4096$ oscillators computed over 10^6 time units after discarding another 10^6 of transient. Red circles correspond to the numerical integration of Eqs. (2) and (3) with a pseudospectral method for 10^5 time units, from which $5 \cdot 10^4$ are transient. Both microscopic and macroscopic simulations use initial conditions close to splay state. Blue crosses correspond to the semi-analytical fixed point given by Eqs. (9) and (10). Black vertical dashed lines indicate the bifurcation points between the different dynamical regimes.
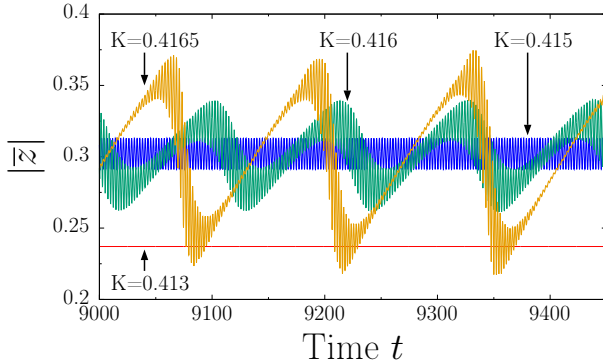

FIG. 3. Time series of $|\bar{z}|$ from the numerical integration of the macroscopic equations of the system for $K = 0.413$ (red), 0.415 (blue), 0.416 (green), and 0.4165 (amber).

not a splay state: only the first Fourier mode vanishes, while the others have non zero amplitude. In other words the distribution of angles is non uniform. The disagreement between microscopic and macroscopic simulations on the bifurcation point K_5 in figure 2 is due to the fact that macroscopic simulations cannot be run long enough for the chaotic transient to finish. Finally, if the coupling is increased even further, one ends up in the highly irregular chaotic regime studied in [14, 31], where the macroscopic equations (2) and (3) are no longer valid, since the oscillators are not distributed along a smooth closed curve.

III. STABILITY OF SPLAY STATE

The macroscopic equations can be used to perform the stability analysis of the splay state by introducing the fields $u(\phi,t)$ and $v(\phi,t)$ which denote infinitesimal perturbations of the probability $P_0 = 1/(2\pi)$ and of the radius $R_0 = \sqrt{1-K}$, respectively. Upon linearizing Eqs. (2) and (3), it is found that

$$v_t = -2(1-K)v + Av_\phi + K \operatorname{Re}[(1+ic_1)\overline{w}\mathrm{e}^{-i\phi}] ,$$

and

$$u_t = Au_\phi + \frac{c_2\sqrt{1-K}}{\pi}v_\phi + \frac{K \operatorname{Re}[(1+ic_1)\overline{w}\mathrm{e}^{-i\phi}]}{2\pi\sqrt{1-K}} ,$$

where

$$A = c_1 K + c_2(1-K)$$

and

$$\overline{w} := \sqrt{1-K}\int_0^{2\pi} d\phi\, u(\phi,t)\,\mathrm{e}^{i\phi} + \frac{1}{2\pi}\int_0^{2\pi} d\phi\, v(\phi,t)\,\mathrm{e}^{i\phi}$$

is the (linear) variation of the mean-field. It is composed of two terms: the former one is the standard Kuramoto-type order parameter, while the latter accounts for fluctuations of the curve $\mathcal{C}$.

The linearized equations can be easily solved in Fourier space, i.e., by introducing

$$\tilde{v}(k,t) = \int_0^{2\pi} d\phi v(\phi,t)\,\mathrm{e}^{ik\phi} \qquad \text{and}$$

$$\tilde{u}(k,t) = \int_0^{2\pi} d\phi u(\phi,t)\,\mathrm{e}^{ik\phi} ,$$

(and the corresponding inverse transforms), since they become block diagonal.

For $k \neq \pm 1$ (including $k = 0$),

$$[\tilde{v}(k)]_t = [-2(1-K) - ikA]\,\tilde{v}(k) \quad \text{and}$$

$$[\tilde{u}(k)]_t = -ik\frac{c_2\sqrt{1-K}}{\pi}\tilde{v}(k) - ikA\tilde{u}(k)$$

so that, the evolution of $\tilde{v}(k)$ is closed onto itself and acts as an external forcing for the dynamics of the probability density, yielding the eigenvalues

$$\lambda_k^{(v)} = -2(1-K) - ik(Kc_1 + c_2(1-K)) \quad \text{and}$$

$$\lambda_k^{(u)} = -ik\,(Kc_1 + c_2(1-K)) .$$

Altogether, the eigenvalues are arranged into two branches: the former corresponds to stable directions associated to the $\mathcal{C}$-dynamics; the latter corresponds to marginally stable directions associated to the density dynamics (this includes the zero mode, whose marginal stability is nothing but a manifestation of probability conservation). Overall the stability of the angle distribution is reminiscent of the marginal stability of the Kuramoto model.
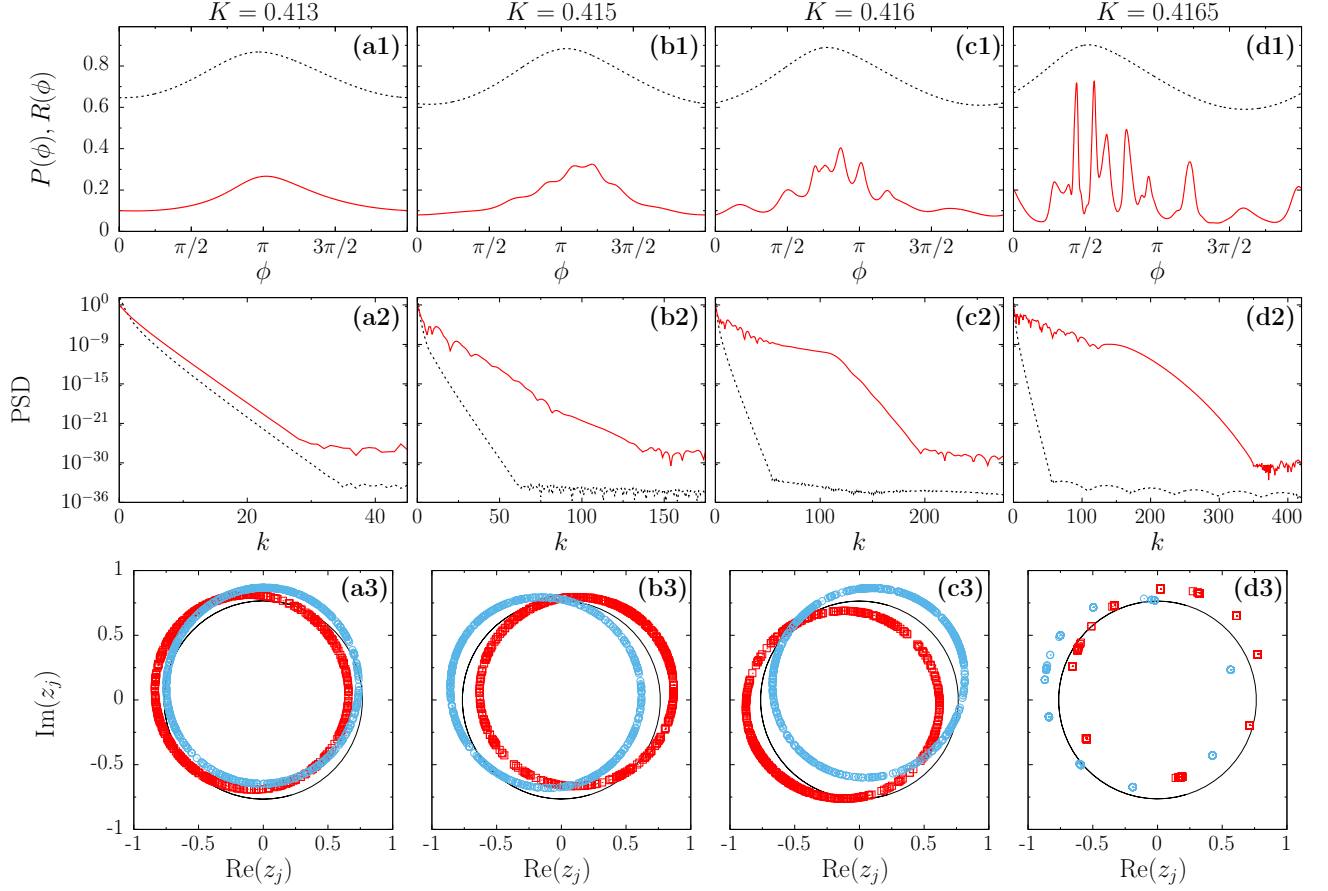
FIG. 4. Snapshots of the shape of R (dashed black curve) and P (red continuous curve) in real space (top row) and the corresponding Power Spectral Density in logarithmic scale (middle row) obtained upon integrating the macroscopic equations using a pseudospectral method. Red squares and blue circles in the bottom row correspond to two snapshots of microscopic simulations with $N = 4096$ taken at different times. Only 512 randomly chosen oscillators are displayed on each panel. Black continuous line correspond to the attracting limit cycle of an uncoupled oscillator, a circle with radius $\sqrt{1 - K}$ centered at the origin. (a1),(a2), and (a3) correspond to $K = 0.413$; (b1), (b2), and (b3) to $K = 0.415$; (c1), (c2), and (c3) to $K = 0.416$; and (d1),(d2), and (d3) to $K = 0.4165$.

The only exception is the first Fourier mode of $v(\phi, t)$, that is coupled back to the shape of the curve. For $k = 1$ we obtain

$$[\tilde{v}(1)]_t = M_{vv}\tilde{v}(1) + M_{vu}\tilde{u}(1) \tag{5}$$
$$[\tilde{u}(1)]_t = M_{uv}\tilde{v}(1) + M_{uu}\tilde{u}(1)$$

where

$$M_{vv} = -2 + \frac{5}{2}K - i\left(A - \frac{Kc_1}{2}\right)$$
$$M_{vu} = -\pi K\sqrt{1-K}(1 + ic_1)$$
$$M_{uv} = \frac{K}{4\pi\sqrt{1-K}} - i\left(\frac{c_2\sqrt{1-K}}{\pi} - \frac{Kc_1}{4\pi\sqrt{1-K}}\right)$$
$$M_{uu} = \frac{K}{2} - i\left(A - \frac{Kc_1}{2}\right).$$

Finally, the equations for $k = -1$ are obtained by simply taking the complex conjugate of the above expressions.

Accordingly, instabilities can and actually do arise within the four-dimensional subspace spanned by the real and imaginary parts of the first modes $\tilde{v}(1)$ and $\tilde{u}(1)$. In practice one needs to determine the stability of the two dimensional complex system (5). Using the Routh–Hurwitz criterion one finds two stability conditions

$$3K < 2, \quad \text{and}$$
$$(2c_1^2 + 8c_1c_2 - c_2^2 + 9)K^2 -$$
$$(c_1^2 + 12c_1c_2 - c_2^2 + 12)K + 4 + 4c_1c_2 < 0$$

In the parameter region considered in this paper, the second inequality reveals a loss of stability for $K > K_1 = (65 - \sqrt{1025})/80 = 0.412304\ldots$, which corresponds to a pair of complex conjugate eigenvalues crossing the imaginary axis, i.e., a Hopf bifurcation. This bifurcation gives rise to SCPS, a periodic collective dynamics, analyzed in the following section. This stability boundary coincides with the one presented in [14] and [16].

IV. SELF-CONSISTENT PARTIAL SYNCHRONY

Above K_1, SCPS does exist and is stable within the region T1. Our general formalism, based on Eqs. (2,3,4), allows performing an analytical study of this regime.

Self-consistent partial synchrony is characterized by a non-uniform probability density, rotating with a collective frequency ω, which differs from the average frequency of the single oscillators. In models where the interactions depend only of phase differences like the present one, ω is constant as well as the amplitude $|\overline{z}|$ of the order parameter. In other words, SCPS corresponds to a fixed point of Eqs. (2,3) in the moving frame $\theta = \phi - \omega t$. Since we are free to choose the origin of the phases, we select a frame where $\overline{z}$ is real and positive, *i.e.*, its phase vanishes (so that from now on we can avoid the use of the absolute value). The equations resulting from this change of variables are

$$R_t = \mathcal{F}[R, \theta, \overline{z}] + \{\omega - \mathcal{G}[R, \theta, \overline{z}]\} R_\theta \tag{6}$$

and

$$P_t = \frac{\partial}{\partial \theta}\Big(P(\theta, t)\{\omega - \mathcal{G}[R, \theta, \overline{z}]\}\Big). \tag{7}$$

accompanied by the self-consistent condition

$$\int_0^{2\pi} d\theta \, P(\theta, t) R(\theta, t) e^{i\theta} =: \overline{z} \, . \tag{8}$$

By imposing the time derivative of R equal to zero in equation (6), we find that the stationary shape of the limit cycle, $R_0(\theta)$, can be obtained by integrating the following ODE,

$$[R_0(\theta)]_\theta = -\frac{\mathcal{F}[R_0, \theta, \overline{z}]}{\omega - \mathcal{G}[R_0, \theta, \overline{z}]} \tag{9}$$

with periodic boundary conditions $R_0(0) = R_0(2\pi)$. The stationary solution P_0 can be thereby obtained by setting the argument of the θ derivative equal to a new unknown constant: minus the probability flux η. The solution reads

$$P_0(\theta) = -\frac{\eta}{\omega - \mathcal{G}[R_0, \theta, \overline{z}]} \, , \tag{10}$$

where η can be obtained from the normalization condition of the probability density $\int_0^{2\pi} P_0 = 1$.

In practice, we proceed as follows. First, we choose putative values for ω and $\overline{z}$, namely ω' and $\overline{z}'$. Making use of such estimates, equation (9) can be solved numerically by means of standard integration methods for boundary value problems, *i.e.* shooting methods [35]. The resulting numerical solution, R_0', can then be replaced in equation (10) to obtain a numerical estimate of P_0, namely P_0'. If ω' and $\overline{z}'$ are the true values for ω and $\overline{z}$ then

$$\int_0^{2\pi} d\theta P_0'(\theta, t) R'(\theta, t) e^{i\theta} = \overline{z}' \, .$$

Recalling that $\overline{z}$ is a real quantity, the problem of solving Eqs. (9) and (10) reduces to finding a fixed point in the $(\omega, \overline{z})$ plane.

The resulting shapes are reported in Figs. 5(a,b) for two different coupling strengths. As expected, both R_0 and P_0 become increasingly nonuniform upon increasing the coupling strength. The blue crosses in Fig. 2, which indicate the values of $|\overline{z}|$ obtained from this approach, agree with the microscopic simulations.

In the rotating frame, where the curve $R(\theta)$ does not depend on time, one can interpret the term in curly brackets in Eq. (7) as the force field acting on an oscillator of phase θ, so that $\mathcal{G}(R(\theta), \theta)$ plays the role of the standard coupling term in ensembles of phase oscillators. The Kuramoto-Sakaguchi model is the simplest setup where the coupling is purely sinusoidal, *i.e.*, $\mathcal{G} = G \sin(\psi + \alpha - \theta)$, where G and ψ are the amplitude and the phase of the order parameter, respectively. In such a case, it is well known that either the splay state or the fully synchronous solution are fully stable, depending whether α is larger or smaller than $\pi/2$. Only for $\alpha = \pi/2$ intermediate macroscopically periodic solutions (SCPS-like) are possible, and, moreover, the dynamics is highly degenerate, since infinitely many solutions exist and are thereby marginally stable. However, as soon as a small second harmonic is added, this high degree of degeneracy is lifted and a finite parameter region appears, where robust SCPS can be observed (see [26]). How do such findings compare with the scenario herein reported for QPOs?

First of all, it should be reminded that the emergence of SCPS in Stuart-Landau oscillators has been already reported in the past (see [22, 25]), a major difference being that the theoretical and numerical studies refer to a parameter region where the single oscillators do not alter their phase character and the coupling manifests itself as a nonlinear dependence on the order parameter and, last but not least, SCPS emerges as a loss of stability of the fully synchronous state.

In the present context, the stability analysis of the splay state reveals that there is no need to include higher harmonics to correctly predict the onset of SCPS, as if they were unnecessary. Since this result conflicts with our general understanding, we have performed a perturbative expansion of the stationary solution in the vicinity of the critical point (see appendix A). The expansion implies that, at leading order, the coupling function $\mathcal{G}$ can be written as the sum of two terms,

$$\mathcal{G} = 2c_2\sqrt{1-K}\, r(\theta) - K\overline{z}\sqrt{\frac{1+c_1^2}{1-K}}\sin(\nu - \theta) \, ,$$

where r is defined in Eq. (A1) and $\nu = \arctan c_1$. Since $r(\theta)$ is itself sinusoidal (see Eq. (A3)), $\mathcal{G}$ is purely sinusoidal as well. The main difference with the Kuramoto-Sakaguchi model is that here there is an additional indirect dependence of the order parameter through the modulation amplitude $r(\theta)$ of $\mathcal{C}$. At criticality, the difference between the phase of the order parameter and that of $r(\theta)$ is $\xi + \nu = -0.1736$, while the difference with the phase of the probability density is $\gamma + \nu = 0.0523$.

At the same time, the perturbative analysis shows also that the amplitude $\overline{z}$ of the order parameter is undetermined at first order. This observation is consistent with the degeneracy exhibited by the Kuramoto-Sakaguchi model at criticality. Moreover, it implies that a second harmonic needs to be

included in the expansion to obtain a full closure of the equations. This is at variance with systems such as the biharmonic model studied in [26], where the shape of the probability density is characterized by the presence of a finite second harmonics from the very beginning. This fact anyway confirms that the presence of second (or higher) harmonics is crucial for the sustainment of SCPS. In the present case such harmonics are spontaneously induced by the modulation of $\mathcal{C}$.

A. Stability analysis of SCPS

Since $(R_0(\theta), P_0(\theta))$ is a fixed point of Eqs. (6) and (7), one can easily study the stability of SCPS by determining the eigenvalues of the corresponding linear operator. Let $v(\theta, t)$ and $u(\theta, t)$ denote an infinitesimal perturbation of $R_0(\theta)$ and $P_0(\theta)$, respectively. By inserting $R(\theta, t) = R_0(\theta) + v(\theta, t)$ and $P(\theta, t) = P_0(\theta) + u(\theta, t)$ into Eqs. (6,7) and retaining only first order terms, we obtain the linear evolution equations,

$$[v(\theta,t)]_t = v(\theta,t)F^{(v)}(\theta) + [v(\theta,t)]_\theta\, G^{(v)}(\theta) \quad (11)$$
$$+ w(t)X^{(v)}(\theta) + \hat{w}(t)Y^{(v)}(\theta)$$

$$[u(\theta,t)]_t = \frac{d}{d\theta}\Big[v(\theta,t)F^{(u)}(\theta) + u(\theta,t)G^{(u)}(\theta) \quad (12)$$
$$+ w(t)X^{(u)}(\theta) + \hat{w}(t)Y^{(u)}(\theta)\Big]$$

where

$$w(t) = \int_0^{2\pi} d\theta e^{i\theta}\,(vP_0 + uR_0) \quad \text{and}$$

$$\hat{w}(t) = \int_0^{2\pi} d\theta e^{-i\theta}\,(vP_0 + uR_0) \quad (13)$$

are the mean-field contributions in tangent space (see appendix B for the definition of the other coefficients). The linear equations are conveniently integrated in Fourier space even though (at variance with the splay state) the change of variables does not diagonalize the problem. It is convenient to work in Fourier space, since one can derive accurate solutions by truncating the infinite series (see the appendix), i.e., by neglecting all modes with $|k| > M$ for some suitably chosen value M. The correct eigenvalues are thereby identified as those that are stable against an increase of M. Additionally, the correctness of the selected values has been double checked by integrating the corresponding eigenvectors (see Eqs. (11,12)). Not unexpectedly, the most relevant eigenvalues (and eigenvectors) do not require large M values.

In figure 5(e) we show the resulting spectra for $K = 0.413$ and 0.414 ($M = 400$ modes have been used in the Fourier expansions). Analogously to the splay state, there are basically two sets of eigenvalues, one having strictly negative real parts, while the other corresponding to almost marginally stable directions (though not strictly vanishing as in the splay state). For $K = 0.413$ all the directions are stable, except for the one corresponding to the phase rotation, while for $K = 0.414$ a
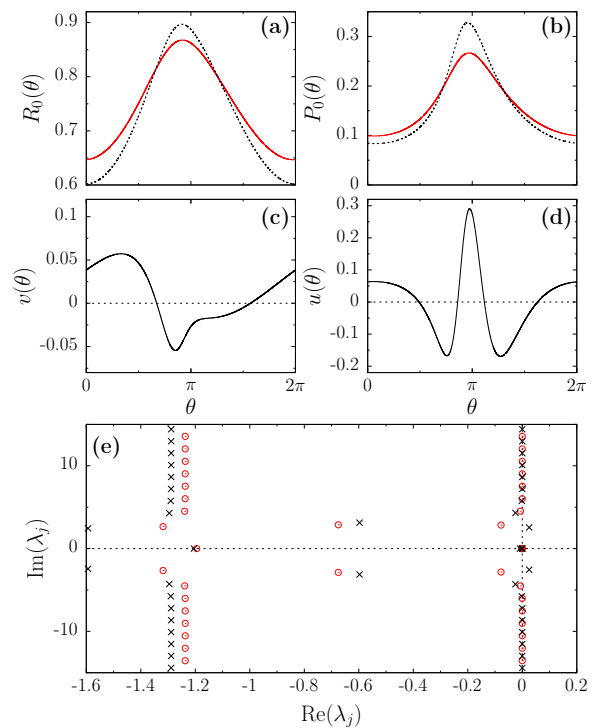

FIG. 5. (a,b) Shapes of $R_0(\theta)$ and P_0 for $K = 0.413$ (red) and 0.414 (black dashed) obtained by solving Eqs. (9,10). (c,d) Shape of the unstable eigenfunction $v(\theta)$ and $u(\theta)$ for $K = 0.414$. (e) Eigenvalues resulting from diagonalizing the linear equations (11) and (12) with $M = 400$ Fourier modes for $K = 0.413$ (red circles) and 0.414 (black crosses).

pair of complex conjugate eigenvalues is present with a positive real part. The corresponding unstable eigenvectors are depicted in Fig. 5(c,d).

Keeping track of such modes for different K values, we can determine the second bifurcation point $K_2 \simeq 0.413765$. Once again this prediction agrees with the microscopic simulations. In Fig. 2, we indeed see that the new regime T2 starts precisely for this value, indicating that the blue crosses obtained for $K > K_2$ correspond to unstable states. According to the stability analysis, the transition appears to be a supercritical Hopf bifurcation. Nevertheless, as it can be read from the phase diagram, in this new regime the limit cycle does not seem to correspond to a rotation around the unstable fixed point (represented by the blue crosses). A detailed analysis of the dynamics of the system close to the bifurcation point shows that the amplitude of the oscillations grows as $\sqrt{K - K_2}$ whereas the frequency does not change significantly. We conjecture that the effect is due to the presence of infinitely many nearly marginal directions, which induce a detachment of the T2 attractor from the plane spanned by the unstable directions of the fixed point.

V. INCREASING DYNAMICAL COMPLEXITY

An analytical study of time-dependent nonlinear regimes is typically unfeasible. So, from now on, we proceed exclusively on a numerical basis, by relying on the integration of both microscopic and macroscopic equations. The Poincaré section is a qualitative but informative tool to understand the dynamical properties of the different regimes observed for larger values of K. It was already used in [30]. Here we consider different observables for reasons that will be clear in a moment. More precisely, we introduce the collective variables

$$Z_n^{(k)} = \left| \int_0^{2\pi} d\psi R(\psi, t_n) P(\psi, t_n) e^{ik\psi} \right|$$

where t_n is the time at which $|\bar{z}|$ reaches a local maximum. This definition is basically an extension of the order parameters typically used to characterize phase oscillators, where the radial contribution R is, for obvious reasons, absent. In phase oscillators, the $Z^{(k)}$ parameters are functionally related to one another whenever the Ott-Antonsen Ansatz is valid [29]. It is therefore instructive to look at their mutual relationship.

In Fig. 6(a), we plot $Z_n^{(1)}$ versus K. Since the Poincaré section reduces by one unit the dimensionality of the underlying attractor, a periodic collective dynamics manifests itself as a single point for a given K value. This is indeed what we see for $K < K_3$, although we should notice that the initial section of the curve corresponds to SCPS, where the order parameter is strictly constant. The fuzzy region covered for $K > K_3$ corresponds to a tiny interval where a T3 dynamics initially unfolds, followed by a chaotic regime, analyzed in more quantitative way in the second part of this section.

The lower panels of Fig. 6 contain various Poincaré section in the T3 region (blue dots) and in the chaotic region (red dots). The points have been obtained by integrating the macroscopic equations. Analogous pictures have been obtained by integrating 32768 oscillators, but significantly blurred by finite-size effects[36]. The main message that we learn by comparing the three Poincaré sections is that there is no functional dependence among the first three order parameters, thus suggesting that they are really independent variables – an indirect evidence that the Watanabe-Strogatz theorem does not apply to this context.

How irregular is the regime which settles beyond K_4? How does chaos emerge? Before proceeding further, it is instructive to stress the conceptual difference between microscopic and macroscopic chaos. The former one manifests itself as irregular fluctuations of local observables such as the amplitude or the phase of a generic oscillator. It is quantified by the "standard" Lyapunov exponents, determined from the linearization of the evolution equations of the single oscillators. Collective chaos is instead associated with fluctuations of macroscopic observables, such as averages over the whole ensemble. It is quantified by the macroscopic Lyapunov exponents, determined from the linearization of the evolution equation of suitable probability densities [37], i.e. after taking the limit $N \to \infty$. How does an order parameter behave in a system with finite N? It typically exhibits a chaotic dynamics
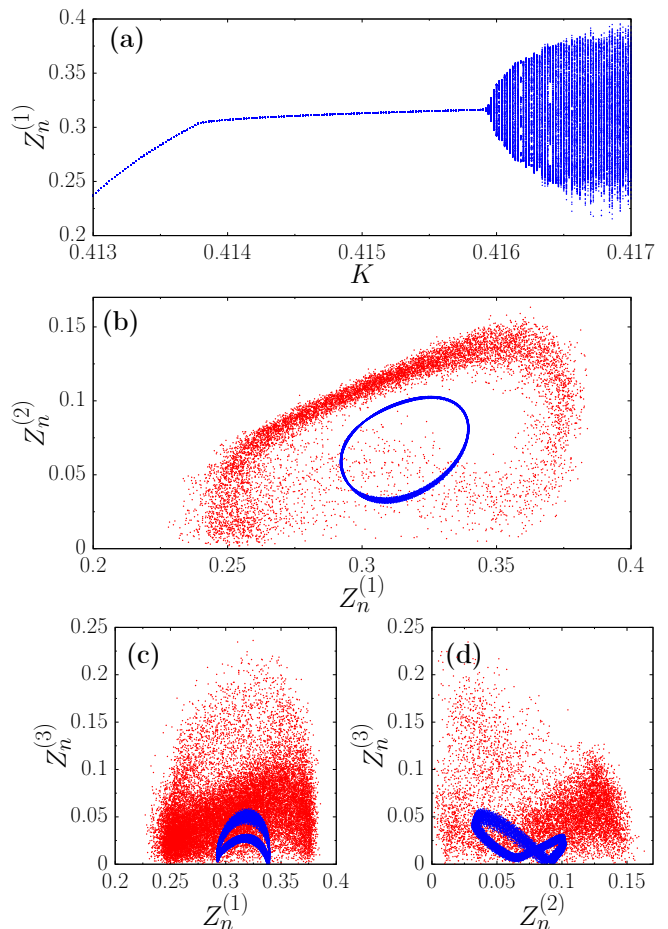

FIG. 6. (a) Poincaré map of $Z_n^{(1)}$ for different values of the coupling strength K computed using macroscopic simulations. The T1 and T2 regimes appear as stable fixed points, and T3 emerges through a Hopf-bifurcation. Simulations computed along 2×10^4 time units after discarding a transient of 5×10^5 time units. (b-d) Poincaré sections resulting from macroscopic simulations for $K = 0.416$ (blue dots) and $K = 0.4165$ (red dots). Simulations computed along 10^5 time units after discarding a transient of 5×10^4 time units.

induced by the nonlinear character of the mutual interactions (see, e.g. [38, 39]). Such fluctuations, however, typically decrease upon increasing N, progressively unearthing the collective dynamics, which can be a fixed point as in the standard Kuramoto model, a limit cycle as in SCPS, or even chaotic as in the present case.

Determining the general scenario in Stuart-Landau oscillators turned out to be arduous. In fact, one has to deal with: (i) long transients; (ii) the spontaneous formation of metastable states; (iii) finite-size effects (in microscopic simulations); (iv) the sporadic formation of highly localized, cluster-like structures (in macroscopic simulations). All of them required much care and long lasting simulations.

We first focus on the computation of the standard, microscopic, Lyapunov exponents. $N = 4096$ turns out to be sufficiently large to ensure negligible finite-size corrections. The convergence is nevertheless very slow and a good way to cope
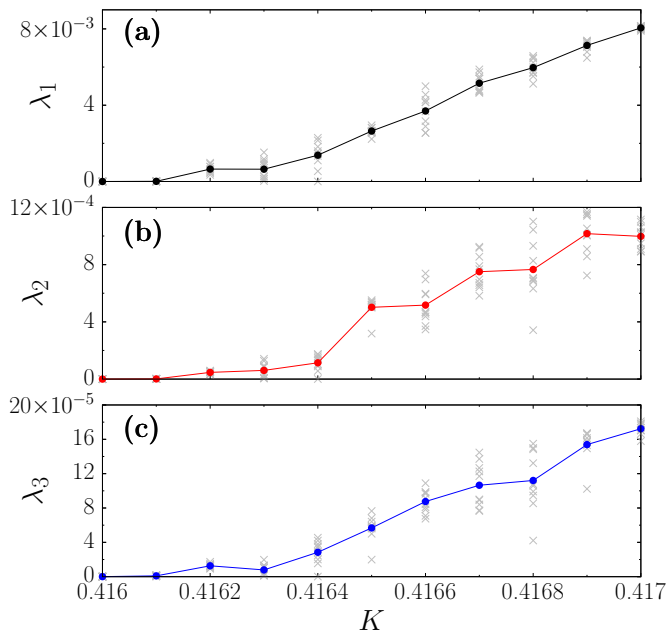
FIG. 7. The three largest Lyapunov exponents of the microscopic system computed over different values of the coupling strength K. Circles indicate the average over ten different realizations, each starting from a different initial condition. Gray crosses show the outcome of the different single realizations. Each simulation consists of $N = 4096$ oscillators, with a quenched disorder of the order of 10^{-14}. The total computation time is of 10^7 time units, of which 10^5 are transient. Simulations computed using fourth order Runge-Kutta with time step $dt = 0.01$. The Gram-Schmidt orthogonalization is invoked every 10 time steps.
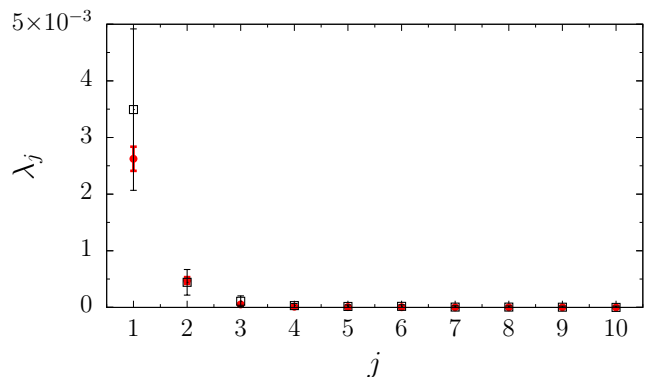

FIG. 8. The ten largest Lyapunov exponents for $K = 0.4165$ computed using microscopic (red circles) and macroscopic (open black squares) simulations. The different points show the average over 10 (microscopic) and 50 (macroscopic) simulations starting from different initial conditions, with error bars indicating the standard deviation. Macroscopic simulations computed over 2×10^4 time units after discarding a transient of 5×10^3. Parameters for microscopic simulations as in figure 7.

with it is by launching simulations from different initial conditions. Moreover, we also add a small heterogeneity of the order of 10^{-14} among the oscillators in order to prevent the formation of spurious clusters due to the finite floating point representation. The parameter dependence of the first three Lyapunov exponents is summarized in Fig. 7. The three exponents appear to become positive for approximately the same coupling strength $K_4 \approx 0.4161\ldots$. This is a first indication that we are before a new transition to chaos. It differs from the typical transitions to low-dimensional chaos (period doubling, intermittency, quasiperiodicity), which are accompanied by the change of sign of a single exponent. On the other hand, there is no similarity with the transitions expected in high-dimensional systems, such as spatio-temporal intermittency, where a bunch of exponents becomes positive, whose numerosity is proportional to the system size [40]: a typical signature of extensivity.

A more detailed representation of the overall degree of instability is given in Fig. 8, where we plot the first ten Lyapunov exponents deeply inside the chaotic region. All exponents beyond the third one are practically equal to zero. As a result, by virtue of the Kaplan-Yorke formula, the underlying attractor is characterized by a large (possibly infinite in the thermodynamic limit) dimension, in spite of the presence of just three positive exponents: an additional reason to classify this regime as genuinely new.

How does the microscopic instability compare to the macroscopic dynamics? In Fig. 8, we plot also the macroscopic Lyapunov exponents, obtained by linearizing the evolution equations (2,3,4) along a generic trajectory. In spite of the large fluctuations (especially those affecting the maximum exponent), the macroscopic spectrum is very similar to the microscopic one. This correspondence is far from obvious and shall be addressed in the final part of this section. Here, we want to stress that the presence of positive macroscopic exponents shows that we are before a form of collective chaos.

In all mean-field models so far investigated in the literature, collective chaos is accompanied by the instability of the single dynamical units, which can be quantified by interpreting the mean field as an external driving force and thereby determining the so-called transverse Lyapunov exponent λ_T. This is the case of logistic maps [41] as well as of Stuart-Landau oscillators in a different parameter region [31]. From now on, we refer to this regime as to *standard collective chaos* (SCC). We now show that the collective dynamics observed beyond $T3$ has a different nature.

In the present context, λ_T can be determined by linearizing the evolution equation (1) under the assumption that $\bar{z}(t)$ is an external forcing,

$$\dot{u} = [1 - K(1 + ic_1)]u - (1 + ic_2)z(2z^*u + zu^*) , \quad (14)$$

where u denotes an infinitesimal perturbation of z. This equation being two-dimensional (u is a complex variable) is characterized by two (transverse) Lyapunov exponents. The lower exponent is unavoidably negative (in the present case it expresses the stability of deviations from the time-dependent curve $\mathcal{C}$). Less trivial is the value of the largest transverse exponent λ_T, which quantifies the stability of perturbations

aligned with the tangent to the curve ($\mathcal{C}$). The best way to describe the underlying phenomenology is by invoking the standard multifractal formalism, which takes into account the fluctuations of the Lyapunov exponents (see, e.g., the book [42]). Let us start by introducing the generalized Lyapunov exponent

$$\mathcal{L}(q) = \lim_{\tau \to \infty} \frac{1}{q\tau} \ln \langle |H(\tau)u|^q \rangle$$

where H represents the Jacobian integrated over a time τ (from Eq. (14)). $\mathcal{L}(0)$ corresponds to the standard Lyapunov exponent, while $\mathcal{L}(1)$ corresponds to the topological entropy (in case there is a single positive exponent) [43]. In fact, $\mathcal{L}(1)$ yields the expansion rate of an *arc* of initial conditions initially aligned along the most expanding direction. In the current context, the orientation of the arc corresponds to that of the curve $\mathcal{C}$. Since the curve itself has a fluctuating but finite length, the length of any subsegment does neither grow nor diverge in time, so that $\mathcal{L}(1) = 0$.

The generalized Lyapunov exponents can be determined from the probability $\mathcal{P}(\Lambda, \tau)$ to observe a finite-time Lyapunov exponent Λ over a time τ and thereby introducing the large deviation function $S(\Lambda)$

$$S(\Lambda) = \lim_{\tau \to \infty} -\frac{\ln \mathcal{P}(\Lambda, \tau)}{\tau} \; .$$

The function $S(\Lambda)$ is equivalent to $\mathcal{L}(q)$, the connection between the two representations being given by the Legendre-Fenchel transform [42]

$$q\mathcal{L}(q) = q\Lambda^* - S(\Lambda^*) \; ,$$

where $q = S'(\Lambda^*)$. In the Gaussian approximation

$$S(\Lambda) = \frac{(\Lambda - \lambda_T)^2}{2D}$$

where λ_T is the standard transverse Lyapunov exponent, while D is the corresponding diffusion coefficient defined as

$$D = \lim_{\tau \to \infty} \tau \left(\overline{\Lambda(\tau)^2} - \lambda_T^2 \right) \; .$$

As a result, we eventually find that

$$\mathcal{L}(1) = \lambda_T + \frac{D}{2} \; . \tag{15}$$

Both λ_T and D can be determined from the time evolution of $\gamma(\tau) = \tau\Lambda(\tau)$[44]. In fact, $\gamma(\tau)$ is the logarithm of the expansion factor over a time τ; it is basically a Brownian motion with a drift velocity λ_T and a diffusion coefficient D. For $K = 0.4165$, upon integrating over 10^7 time units we find a slightly negative Lyapunov exponent $\lambda_T \approx (-1.7 \pm 0.6) \times 10^{-5}$, while $D \approx (4.4 \pm 0.3) \times 10^{-5}$. As a result, from Eq. (15), $\mathcal{L}(1) \approx (0.5 \pm 0.75) \times 10^{-5}$, a value compatible with the expected vanishing exponent. In other words, we see that the fluctuations of the finite-time Lyapunov exponent compensate the slightly negative λ_T and ensure a vanishing expansion factor for the curve length.

Altogether, the message arising from the multifractal analysis is that the (unavoidable) fluctuations of the transverse Lyapunov exponent induce a set of singularities for the corresponding probability density (in the regular SCPS, there are no fluctuations of the Lyapunov exponent, which is identically equal to 0).

A posteriori, this observation accounts for the difficulties encountered in our simulations of the chaotic phase: in fact, the formation of temporary clusters which so much affect the accuracy of our simulations, irrespective whether they are carried out at the microscopic or macroscopic level, are nothing but a manifestation of the unavoidable presence of singularities, which are intrinsically associated to the self-sustainment of a fluctuating probability density.

We conclude this section by commenting on the similarity between macroscopic and microscopic Lyapunov spectra. The correspondence is unexpected since they arise from two different descriptions of the world. In the microscopic approach, the key variables are the "positions" of the single oscillators, while the macroscopic approach deals with their distribution in phase space. Imagine, for simplicity, to deal with N particles constrained to move along a given curve of fixed length: a virtually infinitesimal microscopic perturbation corresponds to a shift of each particle over a scale that is by definition small compared to the interparticle distance, of the order of $1/N$. On the other hand, to meaningfully interpret a perturbation of the positions as a perturbation of the corresponding probability density, it must occur on a scale larger than the statistical fluctuations, which is of order $\sqrt{1/N}$. A priori, there is no guarantee that the linearization of the microscopic equations still hold over such "large scales" (see Ref. [37], for a more detailed discussion of this point). In fact, in typical instances of SCC, macroscopic and microscopic Lyapunov spectra substantially differ from one another. In the toy model of SCC discussed in [37], the collective dynamics is characterized by a single positive macroscopic exponent, while the number of positive exponents is proportional to the number of oscillators, in the microscopic dynamics. The main point of discussion is whether and when some of the microscopic exponents "percolate" to the macroscopic level. In Ref. [31] it is conjectured that this happens whenever the corresponding covariant Lyapunov vector has an extensive nature, but it is still unclear under which conditions this opportunity materializes.

So, what is the difference with the collective chaos discussed in this paper? The stability analysis of splay states in leaky integrate-and-fire (LIF) neurons can help to shed some light. At the collective level, the splay state corresponds to a trivial stationary homogeneous distribution and its stability can be studied by diagonalizing the corresponding linearized evolution operator. This step was already performed in the early'90s, determining an analytical expression of the entire spectrum in the weak coupling limit [45]. More recently, the same problem was revisited from the microscopic point of view, analyzing an arbitrary number N of neurons [46], finding that the leading exponents progressively approach the macroscopic ones (upon increasing N), analogously to what observed in Fig. 8. The main difference between splay states and SCC is the absence of microscopic chaos and thereby the

absence of the statistical fluctuations of size $1/\sqrt{N}$ which would otherwise represent a sort of "barrier" separating the microscopic from the macroscopic world (see [37] for additional considerations of this point). The maintanance of ordering observed in the collective chaos discussed in this paper, makes it closer to the splay state than to SCC.

VI. GENERALITY OF THE QUASI-PHASE OSCILLATORS

In order to prove the generality of the formalism developed in the previous sections, here we investigate a system of globally coupled Rayleigh (van der Pol) [26] oscillators. The equation governing the dynamics the j-th oscillator reads

$$\ddot{x}_j - \zeta(1 - \dot{x}_j^2)\dot{x}_j + x_j = K\,\mathrm{Re}[e^{i\gamma}\overline{x} + i\overline{y}] \qquad (16)$$

where ζ and γ are system parameters, K is the coupling strength, and $\overline{x}$ and $\overline{y}$ are mean-field variables,

$$\overline{x} = \frac{1}{N}\sum_{m=1}^{N} x_m \quad \text{and} \quad \overline{y} = \frac{1}{N}\sum_{m=1}^{N} \dot{x}_m .$$

For $\zeta = 5$, an uncoupled unit of the system is strongly attracted to a limit-cycle. As reported in previous works [26], for a coupling strength $K = 0.05$ and upon varying γ, the system displays a wide range of regimes, including periodic SCPS and different types of clustered states. All such regimes can be described in terms of an equivalent Kuramoto-Daido phase model obtained through usual phase reduction techniques [26]. Here we show that upon increasing the coupling strength to $K = 0.1$ the oscillators arrange themselves along a time-varying closed curve, as illustrated by the snapshots of figure 9(a).

Analogously to the Stuart-Landau setup, this behavior can be described in terms of macroscopic equations. Since the origin $(0,0)$ falls in the center of the limit cycle, it is convenient to introduce the complex variable $z_j := x_j + iy_j = r_j e^{i\phi_j}$ and express Eq. (16) in polar coordinates obtaining

$$\dot{r}_j = \hat{\mathcal{F}}[r_j, \phi_j, \overline{z}]$$
$$\dot{\phi}_j = \hat{\mathcal{G}}[r_j, \phi_j, \overline{z}] ,$$

where

$$\hat{\mathcal{F}}[r, \phi, \overline{z}] = \zeta r \sin^2(\phi)(1 - r^2\sin^2(\phi))$$
$$+ K\sin(\theta)\left(X\cos(\gamma) - Y\sin(\gamma)\right)$$
$$\hat{\mathcal{G}}[r, \phi, \overline{z}] = -1 + \zeta\sin(\phi)\cos(\phi)(1 - r^2\sin^2(\theta))$$
$$+ K\sin(\theta)\left(X\cos(\gamma) - Y\sin(\gamma)\right) ,$$

and $\overline{z} = \overline{x} + i\overline{y}$. This way, the macroscopic equations have the same structure as for the Stuart-Landau oscillators (see Eqs. (2,3,4)), the only difference being that the velocity fields $\mathcal{F}$ and $\mathcal{G}$ are replaced by $\hat{\mathcal{F}}$ and $\hat{\mathcal{G}}$, respectively.

The correctness of the macroscopic approach is confirmed in Fig. 9(b), where the evolution of the order parameter obtained from the integration of the microscopic equations (red

circles) is superposed to the outcome of Eq. (16) (black curve). The closure of the curve shows that, for this set of parameters, the collective dynamics is periodic. On the other hand, the non-circular structure reveals that the modulus of the order parameter oscillates (periodically), i.e. that this regime is of the same type of T2 observed in the Stuart-Landau oscillators.

In order to quantify the oscillations of the closed curve, we identify its leftmost and rightmost points,

$$x_L(t) := \min_\phi\left(R(\phi, t)\cos(\phi)\right) \quad \text{and}$$
$$x_R(t) := \max_\phi\left(R(\phi, t)\cos(\phi)\right) ,$$

and thereby define the x-center of the curve as $\hat{x}(t) := (x_L + x_R)/2$. The resulting oscillations, presented in Figure 9(c), provide a quantitative representation of the curve dynamics.

A more detailed view of the collective regime is presented in Fig. 9(d), where we report three snapshots of the probability density $P(\phi, t)$ at three different times (see the solid curves), which reveal substantial differences. To what extent such fluctuations are a consequence of our definition of ϕ? In order to investigate this point, we have introduced the more meaningful definition of phase,

$$\theta = 2\pi\frac{T_\phi^0}{T} ,$$

where T_ϕ^0 denotes the time for an uncoupled oscillator to travel from the point with phase ϕ to the origin [47], while T is the total period. The resulting $\theta(\phi)$ is plotted in the inset of Fig. 9(d), while the corresponding probability densities correspond to the dashed lines in the body of the figure. The tiny differences between the two representations confirm that the strong shape changes of the probability density is a true macroscopic effect.

VII. CONCLUSIONS AND OPEN PROBLEMS

In this paper we have discussed a regime, where the single oscillators maintain some phase-like properties (e.g., the alignment along a closed curve $\mathcal{C}$), but their amplitude plays a non trivial role, by inducing fluctuations of the curve itself. As a result, one can still parametrize a population of oscillators in terms of a probability density of their phases, but, at variance with standard phase oscillators, it is necessary to include a second PDE to account for the dynamics of $\mathcal{C}$, along which the oscillators are distributed.

The QPO regime is a fairly general regime: for the sake of simplicity, we mostly focused on Stuart-Landau oscillators, but the analysis of Rayleigh oscillators, carried over in the previous section, shows that the approach is general and applications are possible in all contexts where synchronization of oscillators is currently scrutinized. Computational neuroscience is a particularly promising area, since often neurons are treated as phase oscillators, but it is also clear that this is just an approximation. Interestingly, a regime akin to T2
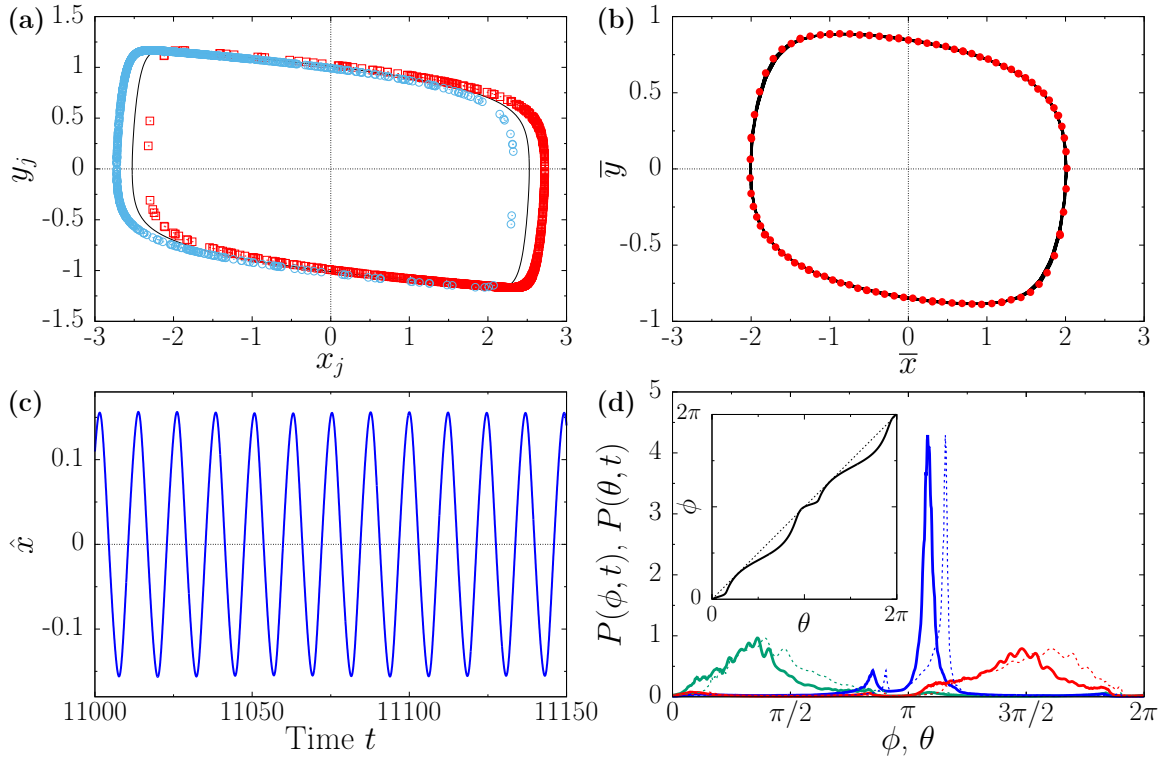
FIG. 9. Dynamics of the Rayleigh system (see Eq. (16)) with $\zeta = 5$, $\gamma = -0.1$, and $K = 0.1$. (a) Red squares and blue circles correspond to two different snapshots of microscopic simulations of the Rayleigh system with $N = 1000$ oscillators. Black curve corresponds to the limit cycle of a single uncoupled oscillator. (b) Limit-cycle trajectory displayed by the order parameter obtained by integrating the macroscopic (black curve) and microscopic (red circles) equations respectively. (c) Time series of the horizontal displacement of the curve, Δx. (d) Purple, red, and blue curves correspond to snapshots of the probability density $P(\phi, t)$ taken at three different times. Results obtained by integrating the macroscopic equations with pseudospectral method.

has been recently observed in quadratic integrate-and-fire neurons, in the presence of delay [48]. Therein, because of the delay, the neurons automatically behave as (quasi)amplitude oscillators: it will be instructive to revisit the setup from the point of view proposed in the present paper.

The expected generality of the phenomenology, together with the evidence that different "phase" parametrizations are formally equivalent suggest the possibility to construct a sort of normal form, valid for different model (at least in the vicinity of the bifurcations). We envisage the perspective of a sort of generalized Kuramoto-Daido model, which includes the curve dynamics.

From the point of view of the dynamical regimes, we confirm that SCPS is a generic regime. We already knew that more than one Fourier harmonics are required for the self-sustainment of SCPS: here we find that the onset of additional harmonics is ensured by the amplitude dynamics. Our formalism allows for an almost analytical characterization of SCPS and, in particular, to determine the bifurcation point, beyond which complex time-dependent states arise. If SCPS is by itself a non-intuitive regime, since the single oscillators behave quasi-periodically without displaying any locking phenomena, the chaotic SCPS described in section V is even more so. Each oscillator, under the action of the self-sustained chaotic

mean-field, is consistently marginally stable (the transversal generalized Lyapunov exponent being equal to zero for $q = 1$) when the coupling strength is varied. An implication of this observation is that the probability density is unavoidably characterized by the presence of singularities that manifest themselves as temporary clusters.

If and when the transversal Lyapunov exponent becomes positive, a transition to SCC occurs, accompanied by the divergence of the curve $\mathcal{C}$, which would thereby "fill" the phase space (in a fractal way). In the parameter range explored in this paper, this transition is preceded by the onset of a non-conventional incoherent state (i.e. nonuniform distribution characterized by a zero order parameter), which restores a perfectly circular shape of $\mathcal{C}$. It will be worth clarifying the possibly universal mechanisms that may lie behind such a kind of transition.

Finally, the onset of a chaotic SCPS is itself an entirely new phenomenon which involves the simultaneous emergence of more than one positive Lyapunov exponent (actually it looks like three of them). While we could imagine simple mechanisms for the emergence of discontinuous changes (see, e.g. attractor crises), the justification of a continuous transition such as the one discussed in this paper is by far more intriguing. Last but not least, the question whether chaotic SCPS can

be observed in perfect phase oscillators remains open.

Appendix A: First order approximation of SCPS

In this section we develop a perturbative approach to determine the stationary solutions of Eqs. (9,10) close to the transition to SCPS, $K \sim K_1$. The main idea is, as usual, the identification of the leading terms. Slightly above K_1, the shape R_0 of the attractor and the corresponding density distribution P_0 of the phases are close to the splay state, so that we can write

$$R_0(\theta) = \sqrt{1 - K} + r(\theta) \qquad (A1)$$
$$P_0(\theta) = \frac{1}{2\pi} + p(\theta) \ .$$

Expanding the self-consistent condition (8) up to linear terms, we obtain

$$\bar{z} = \int_0^{2\pi} d\psi P(\psi) R(\psi) e^{i\psi}$$
$$= \frac{1}{2\pi} \int_0^{2\pi} e^{i\psi} d\psi r(\psi) + \sqrt{1-K} \int_0^{2\pi} d\psi p(\psi) e^{i\psi}$$
$$= \frac{1}{2\pi} \tilde{r}(1) + \sqrt{1-K} \tilde{p}(1) \ . \qquad (A2)$$

By then expanding equation (9) up to first order, one obtains

$$[r(\theta)]_\theta = \frac{2(1-K)r - K\bar{z}\sqrt{1+c_1^2}\cos(\nu-\theta)}{\Delta} \ ,$$

where

$$\Delta := \omega + c_1 K + c_2(1-K) \ ,$$
$$\nu := \arctan c_1$$

By introducing the notations

$$a_\xi e^{i\xi} := \frac{2(1-K)}{\Delta} - i,$$
$$A := \frac{K\sqrt{1+c_1^2}}{a_\xi \Delta},$$

one can write the solution of the ODE as

$$r(\theta) = \bar{z} A \cos(\nu + \xi - \theta) \ . \qquad (A3)$$

Accordingly,

$$\tilde{r}(1) = \pi \bar{z} A e^{i(\nu+\xi)}$$

By expanding Eq. (10) in the same way, at zero order we obtain

$$\eta = -\frac{\Delta}{2\pi}$$

while, at first order,

$$p(\theta) = \frac{-2c_2(1-K)r(\theta) + K\bar{z}\sqrt{1+c_1^2}\sin(\nu-\theta)}{2\pi\Delta\sqrt{1-K}}$$

By replacing the expression for $r(\theta)$,

$$p(\theta) = C\bar{z}\left[-\frac{2c_2(1-K)}{a_\xi \Delta}\cos(\nu+\xi-\theta) + \sin(\nu-\theta)\right]$$

where

$$C = \frac{K}{2\pi\Delta}\sqrt{\frac{1+c_1^2}{1-K}} \ .$$

By finally, recombining the two sinusoidal terms, we find

$$p(\theta) = a_\gamma C\bar{z}\cos(\nu+\gamma-\theta)$$

where

$$a_\gamma e^{i\gamma} = \frac{-2(1-K)c_2 e^{i\xi}}{a_\xi \Delta} - i \ .$$

Thus, also $p(\theta)$ is a purely harmonic function and

$$\tilde{p}(1) = \pi\bar{z}a_\gamma C e^{i(\nu+\gamma)} \ .$$

The overall effect of the coupling is finally determined by inserting the expressions for $\tilde{r}(1)$ and $\tilde{p}(1)$ into Eq. (A2). Since both terms are proportional to $\bar{z}$, we can interpret

$$G := g_z e^{i\delta} := \frac{A}{2}e^{i(\xi+\nu)} + \pi a_\gamma C\sqrt{1-K}e^{i(\gamma+\nu)} \ ,$$

as the expansion factor of $\bar{z}$ in the presence of a given small modulation of both $\mathcal{C}$ and the probability density. Imposing $G = 1$ finally allows determining a self-consistent solution. More precisely, one can determine the frequency ω of the collective rotation (so far unspecified) and the bifurcation point K. For $c_1 = -2$ and $c_2 = 3$, we obtain $K = K_1 \simeq 0.4123...$ and $\omega = \omega_c = -2.5261...$, i.e., in agreement with the stability analysis of the splay state.

Appendix B: Stability of SCPS

The coefficients of the linearized equations (11,12) are

$$F^{(v)}(\theta) := (1 - K) - 3R_0(\theta)^2 + 2c_2 R_0'(\theta)R_0(\theta)$$
$$+ \frac{K\bar{z}R_0'(\theta)}{R_0^2(\theta)}\sqrt{1 + c_1^2}\sin(\nu - \theta)\,,$$

$$G^{(v)}(\theta) := Kc_1 + \omega + c_2 R_0^2 - \frac{K\bar{z}}{R_0(\theta)}\sqrt{1 + c_1^2}\sin(\nu - \theta)\,,$$

$$X^{(v)}(\theta) := \frac{K\sqrt{1 + c_1^2}}{2}\left(1 - \frac{R_0'(\theta)}{iR_0(\theta)}\right)e^{i(\nu - \theta)}\,,$$

$$Y^{(v)}(\theta) := \frac{K\sqrt{1 + c_1^2}}{2}\left(1 + \frac{R_0'(\theta)}{iR_0(\theta)}\right)e^{-i(\nu - \theta)}\,,$$

$$F^{(u)}(\theta) := 2c_2 P_0(\theta)R_0(\theta) + \frac{KP_0(\theta)\bar{z}}{R_0(\theta)^2}\sqrt{1 + c_1^2}\sin(\nu - \theta)\,,$$

$$G^{(u)}(\theta) := Kc_1 + \omega + c_2 R_0(\theta)^2 - \frac{K\bar{z}}{R_0(\theta)}\sqrt{1 + c_1^2}\sin(\nu - \theta)\,,$$

$$X^{(u)}(\theta) := -\frac{KP_0(\theta)}{2iR_0(\theta)}\sqrt{1 + c_1^2}e^{i(\nu - \theta)}\,,$$

$$Y^{(u)}(\theta) := \frac{KP_0(\theta)}{2iR_0(\theta)}\sqrt{1 + c_1^2}e^{-i(\nu - \theta)}\,.$$

The equations are better solved in Fourier space. By invoking the Fourier transform, the integrals in the linearized mean-field expression (13) can be expanded as a linear combination of $\{\tilde{v}(k,t)\}_{k=-\infty}^{\infty}$ and $\{\tilde{u}(k,t)\}_{k=-\infty}^{\infty}$,

$$w(t) = \frac{1}{2\pi}\sum_{k=-\infty}^{\infty}\tilde{v}(k)\tilde{P}_0(1 - k) + \tilde{u}(k)\tilde{R}_0(1 - k)$$

and

$$\hat{w}(t) = \frac{1}{2\pi}\sum_{k=-\infty}^{\infty}\tilde{v}(k)\tilde{P}_0(-1 - k) + \tilde{u}(k)\tilde{R}_0(-1 - k).$$

Similarly, we express Eqs. (11) and (12) in Fourier space. Retaining the terms for each wavelength k we obtain an infinite system of linear equations,

$$[\tilde{v}(k)]_t = \frac{1}{2\pi}\sum_{j=-\infty}^{\infty}\tilde{v}(j)\Big[\tilde{F}^{(v)}(k - j) - ij\tilde{G}^{(v)}(k - j)$$
$$+ \tilde{X}^{(v)}(k)\tilde{P}_0(1 - j) + \tilde{Y}^{(v)}(k)\tilde{P}_0(-1 - j)\Big]$$
$$+ \tilde{u}(j)\Big[\tilde{X}^{(v)}(k)\tilde{R}_0(1 - j) + \tilde{Y}^{(v)}(k)\tilde{R}_0(-1 - j)\Big]$$

and

$$[\tilde{u}(k)]_t = \frac{-ik}{2\pi}\sum_{j=-\infty}^{\infty}\tilde{v}(j)\Big[\tilde{F}^{(u)}(k - j)$$
$$+ \tilde{X}^{(u)}(k)\tilde{P}_0(1 - j) + \tilde{Y}^{(u)}(k)\tilde{P}_0(-1 - j)\Big]$$
$$+ \tilde{u}(j)\Big[\tilde{G}^{(u)}(k - j) + \tilde{X}^{(u)}(k)\tilde{R}_0(1 - j)$$
$$+ \tilde{Y}^{(u)}(k)\tilde{R}_0(-1 - j)\Big]\,.$$

[1] The term "collective" is often used to refer to the behavior of an ensemble of units induced by mutual coupling. Here we use it to refer, as in statistical-mechanics, to macroscopic features exhibited by observables averaged over a formally infinite number of contributions.

[2] Peter Richard, Barbara M. Bakker, Bas Teusink, K Van Dam, and Hans Westerhoff, "Acetaldehyde mediates the synchronization of sustained glycolytic oscillations in populations of yeast cells," European journal of biochemistry / FEBS **235**, 238–41 (1996).

[3] István Z. Kiss, Yumei Zhai, and John L. Hudson, "Emerging coherence in a population of chemical oscillators," Science **296**, 1676–1678 (2002), http://science.sciencemag.org/content/296/5573/1676.full.pdf.

[4] Erik Andreas Martens, Shashi Thutupalli, Antoine Fourrière, and Oskar Hallatschek, "Chimera states in mechanical oscillator networks," Proceedings of the National Academy of Sciences **110**, 10563–10567 (2013), https://www.pnas.org/content/110/26/10563.full.pdf.

[5] Kenichi Hirosawa, Seiichi Kittaka, Yu Oishi, Fumihiko Kannari, and Takayuki Yanagisawa, "Phase locking in a nd:yvo4 waveguide laser array using talbot cavity," Optics express **21**, 24952–61 (2013).

[6] A Vladimirov, G Kozyreff, and Mandel , "Synchronization of weakly stable oscillators and semiconductor laser arrays," EPL (Europhysics Letters) **61**, 613 (2007).

[7] K. Segall, M. LeGro, S. Kaplan, O. Svitelskiy, S. Khadka, P. Crotty, and D. Schult, "Synchronization dynamics on the picosecond time scale in coupled josephson junction neurons," Phys. Rev. E **95**, 032220 (2017).

[8] Shandelle Henson, James Hayward, Jim Cushing, and Joseph Galusha, "Socially induced synchronization of every-other-day egg laying in a seabird colony," The Auk **127**, 571–580 (2010).

[9] D C Michaels, E P Matyas, and J Jalife, "Mechanisms of sinoatrial pacemaker synchronization: a new hypothesis." Circulation Research **61**, 704–714 (1987).

[10] D. Golomb, D. Hansel, B. Shraiman, and H. Sompolinsky, "Clustering in globally coupled phase oscillators," Phys. Rev. A **45**, 3516–3530 (1992).

[11] Y. Kuramoto and D. Battogtokh, "Coexistence of coherence and incoherence in nonlocally coupled phase oscillators," Nonlinear Phenomena in Complex Systems **5**, 180 (2002).

[12] Daniel M. Abrams and Steven H. Strogatz, "Chimera states for coupled oscillators," Phys. Rev. Lett. **93**, 174102 (2004).

[13] Kunihiko Kaneko, "Globally coupled chaos violates the law of large numbers but not the central-limit theorem," Phys. Rev. Lett. **65**, 1391–1394 (1990).

[14] Naoko Nakagawa and Yoshiki Kuramoto, "Collective chaos in

a population of globally coupled oscillators," Progress of Theoretical Physics **89**, 313 (1993).

[15] Wouter-Jan Rappel Vincent Hakim, "Dynamics of the globally coupled complex ginzburg-landau equation," Physical Review A **46**, 7347–7350 (1992).

[16] Wouter-Jan Rappel Marie-Line Chabanol, Vincent Hakim, "Collective chaos and noise in the globally coupled complex ginzburg-landau equation," Physica D **103**, 273–293 (1997).

[17] Diego Pazó and Ernest Montbrió, "From quasiperiodic partial synchronization to collective chaos in populations of inhibitory neurons with delay," Phys. Rev. Lett. **116**, 238101 (2016).

[18] S. Olmi, A. Politi, and A. Torcini, "Collective chaos in pulse-coupled neural networks," EPL (Europhysics Letters) **92**, 60007 (2010).

[19] Stefano Luccioli and Antonio Politi, "Irregular collective behavior of heterogeneous neural networks," Phys. Rev. Lett. **105**, 158104 (2010).

[20] C. van Vreeswijk, "Partial synchronization in populations of pulse-coupled oscillators," Phys. Rev. E **54**, 5522–5537 (1996).

[21] P.K. Mohanty and A. Politi, "A new approach to partial synchronization in globally coupled rotators," J. Phys. A: Math. Gen. **39**, L415–L421 (2006).

[22] Michael Rosenblum and Arkady Pikovsky, "Self-organized quasiperiodicity in oscillator ensembles with global nonlinear coupling," Phys. Rev. Lett. **98**, 064101 (2007).

[23] Arkady Pikovsky and Michael Rosenblum, "Self-organized partially synchronous dynamics in populations of nonlinearly coupled oscillators," Physica D: Nonlinear Phenomena **238**, 27 – 37 (2009).

[24] Antonio Politi and Michael Rosenblum, "Equivalence of phase-oscillator and integrate-and-fire models," Phys. Rev. E **91**, 042916 (2015).

[25] M. Rosenblum and A. Pikovsky, "Two types of quasiperiodic partial synchrony in osciliator ensembles," Phys. Rev. E **92**, 012919 (2015).

[26] Pau Clusella, Antonio Politi, and Michael Rosenblum, "A minimal model of self-consistent partial synchrony," New Journal of Physics **18**, 093037 (2016).

[27] A. Torcini E. Ullner, A. Politi, "Ubiquity of collective irregular dynamics in balanced networks of spiking neurons," CHAOS **28**, 081106 (2018).

[28] S. Watanabe and S. H. Strogatz, "Integrability of a globally coupled oscillator array," Phys. Rev. Lett. **70**, 2391–2394 (1993).

[29] Edward Ott and Thomas M. Antonsen, "Low dimensional behavior of large systems of globally coupled oscillators," Chaos **18**, 037113 (2008).

[30] Naoko Nakagawa and Yoshiki Kuramoto, "Anomalous lyapunov spectrum in globally coupled oscillators," Physica D: Nonlinear Phenomena **80**, 307 – 316 (1995).

[31] Kazumasa A Takeuchi and Hugues Chaté, "Collective lyapunov modes," Journal of Physics A: Mathematical and Theoretical **46**, 254007 (2013).

[32] H. Sakaguchi and Y. Kuramoto, "A soluble active rotator model showing phase transition via mutual entrainment," Prog. Theor. Phys. **76**, 576–581 (1986).

[33] Gautam C. Sethia and Abhijit Sen, "Chimera states: The existence criteria revisited," Phys. Rev. Lett. **112**, 144101 (2014).

[34] C. Canuto, M.Y. Hussaini, A. Quarteroni, and Th.A. Zang, *Spectral Methods: Fundamentals in Single Domains*, 1st ed., Can (Springer-Verlag, Berlin, 2006) Chap. 2.

[35] J. Stoer, R. Bartels, W. Gautschi, R. Bulirsch, and C. Witzgall, *Introduction to Numerical Analysis*, Texts in Applied Mathematics (Springer New York, 2013).

[36] The obfuscation of blue points clearly visible in panels (c) and (d) of Fig. 6 are also artifacts due to the finite accuracy in the determination of the Poincaré section.

[37] Antonio Politi, Arkady Pikovsky, and Ekkehard Ullner, "Chaotic macroscopic phases in one-dimensional oscillators," The European Physical Journal Special Topics **226**, 1791–1810 (2017).

[38] Oleksandr V. Popovych, Yuri L. Maistrenko, and Peter A. Tass, "Phase chaos in coupled oscillators," Phys. Rev. E **71**, 065201 (2005).

[39] Christian Bick, Marc Timme, Danilo Paulikat, Dirk Rathlev, and Peter Ashwin, "Chaos in symmetric phase oscillator networks," Physical review letters **107**, 244101 (2011).

[40] Hugues Chaté and Paul Manneville, "Transition to turbulence via spatio-temporal intermittency," Phys. Rev. Lett. **58**, 112–115 (1987).

[41] Tatsuo Shibata and Kunihiko Kaneko, "Tongue-like bifurcation structures of the mean-field dynamics in a network of chaotic elements," Physica D: Nonlinear Phenomena **124**, 177 – 200 (1998).

[42] Arkady Pikovsky and Antonio Politi, *Lyapunov Exponents: A Tool to Explore Complex Dynamics* (Cambridge University Press, 2016).

[43] We warn the reader that a different definition is often found in the literature, where $q = 1$ corresponds to the standard Lyapunov exponent. Here we follow the same notations as in [42].

[44] Here, $\Lambda(\tau)$ denotes the finite-time Lyapunov exponent computed by following a single trajectory from time 0 to time τ.

[45] L. F. Abbott and Carl van Vreeswijk, "Asynchronous states in networks of pulse-coupled oscillators," Phys. Rev. E **48**, 1483–1490 (1993).

[46] Simona Olmi, Antonio Politi, and Alessandro Torcini, "Linear stability in networks of pulse-coupled neurons," Frontiers in Computational Neuroscience **8**, 8 (2014).

[47] This is because the oscillators rotate clockwise.

[48] Federico Devalle, Ernest Montbrió, and Diego Pazó, "Dynamics of a large system of spiking neurons with synaptic delay," Phys. Rev. E **98**, 042214 (2018).